The Astrophysical Journal, 647:676–684, 2006 August 10

SIGNATURES OF THE *s*-PROCESS IN PRESOLAR SILICON CARBIDE GRAINS: BARIUM THROUGH HAFNIUM

Qing-Zhu Yin
Department of Geology, University of California, Davis, CA 95616; yin@geology.ucdavis.edu

Cin-Ty Aeolus Lee
Department of Earth Sciences, Rice University, Houston, TX 77005; ctlee@rice.edu

and

Ulrich Ott[1]
Max-Planck-Institut für Chemie, Becherweg 27, D-55128 Mainz, Germany; ott@mpch-mainz-mpg.de
Received 2005 December 5; accepted 2006 April 6

ABSTRACT

Isotopic and elemental abundance signatures in the mass range Ba through Hf have been determined in a silicon carbide–rich sample of the Murchison carbonaceous chondrite, using inductively coupled plasma mass spectrometry (ICP-MS). Despite the problem of some isobaric interferences, useful results were obtained for a number of isotopes. Disagreements between astrophysical predictions and previous results for ^{137}Ba and ^{146}Nd obtained by thermal ionization mass spectrometry are confirmed. Our data for Dy are more in line with predictions, however. The *s*-process signatures for several other elements in the rare earth element (REE) mass range were observed for the first time and are also consistent with theoretical predictions. The elemental abundance pattern shows deficit relative to production ratios of the more volatile REE, notably Yb, and, to a lesser extent, Sm and Eu. This may allow estimating an average condensation temperature of trace elements into SiC.

Subject headings: meteors, meteoroids — nuclear reactions, nucleosynthesis, abundances — stars: AGB and post-AGB — stars: carbon

1. INTRODUCTION

Primitive meteorites are a rich source of pristine presolar grains that formed in stellar atmospheres and ejecta and have survived travel through the interstellar medium as well as the process of solar system formation (Anders & Zinner 1993; Ott 1993; Bernatowicz & Zinner 1997). Their study in the laboratory constitutes a link between astrophysics, cosmochemistry and meteorite research. Although abundant in the interstellar medium (e.g., Draine 2003; Whittet 2003), presolar silicates have only recently been proven to be present in both interplanetary dust particles (Messenger et al. 2003) and meteorites (Nguyen & Zinner 2004; Mostefaoui & Hoppe 2004). Most of the grain types detected earlier are characterized by being extremely refractory and chemically resistant minerals such as diamond, graphite, silicon carbide, silicon nitride, and various refractory oxides (e.g., Zinner 1998).

Grains of silicon carbide (SiC) have been studied most extensively for a variety of reasons. First, they are relatively abundant (up to 30 ppm in the Murchison meteorite; e.g., Ott & Merchel 2000). Furthermore, all of them are presolar (Hoppe & Ott 1997) and are large enough (tenths of to several μm) that the isotopic composition of many elements can be studied by modern secondary ion mass spectrometry (SIMS) instruments like the NanoSIMS (e.g., Hoppe et al. 2004). Finally, they contain a rich trove of trace elements above $A = 80$ with *s*-process signatures, which can shed detailed light on nucleosynthesis processes in the parent asymptotic giant branch (AGB) stars. In fact, the *s*-process Kr and Xe contained within SiC grains (Lewis et al. 1990; Hoppe & Ott 1997) was one of the crucial pieces of evidence establishing the very existence of presolar matter in solar system objects.

The first analyses of elements in SiC showing signatures of the *s*-process (other than Kr and Xe) were made on aggregates of (many) SiC grains by thermal ionization mass spectrometry (TIMS) and by SIMS (Ott & Begemann 1990a, 1990b; Zinner et al. 1991; Prombo et al. 1993). For a summary of these results that were obtained for the elements Sr, Ba, Nd, Sm, and Dy, see Hoppe & Ott (1997). The study of single grains for the more abundant *s*-process elements was made possible with the development of resonance ionization mass spectrometry (RIMS) by Günther et al. (1997) and applied to the study of Sr, Zr, Mo, Ru, and Ba (Nicolussi et al. 1997, 1998a, 1998b; Savina et al. 2003, 2004). Because of its relatively high abundance and good ionization yield, it has also been possible to analyze Ba in single SiC grains with the NanoSIMS (Marhas et al. 2003, 2005).

Almost all of these isotopic analyses of *s*-process elements, whether on single grains or aggregates, were (apart from measurements of the major elements) basically one-element studies. Here, we report on the application of yet another technique, inductively coupled plasma mass spectrometry (ICP-MS), a multielement technique that has allowed us to obtain data in the mass range from Ba to Hf. A drawback of the method is the fact that in analyses of multielement samples there are abundant isobaric interferences in the region of the rare earth elements (REEs). In fact, isobaric interference is the outcome in those interesting cases where there are branchings in the *s*-process. Nevertheless, our results for the subset of isotopic pairs that are free from interferences or where corrections can be applied with confidence provide valuable information on the *s*-process contribution to many *s*-process elements. By necessity, our ICP-MS measurements were performed on many grains (i.e., a slurry aggregate), hence the results presented here should provide a representative average pattern of the *s*-process in presolar SiC between Ba and Hf. Notably, this includes not only isotopic

[1] Corresponding author.

compositions, but also the elemental abundance pattern over a wide mass range.

The results reported here were obtained in an experiment originally aimed at analyzing trace elements in Murchison nanodiamonds rather than SiC. As it turned out, indigenous trace elements in diamonds are exceedingly rare (Merchel et al. 2003), while *s*-process elements in SiC are abundant. As a consequence, the small SiC impurities in the diamond separates dominated the trace element pattern in the Ba to REE region.

2. EXPERIMENTAL

2.1. *Sample*

The analyzed acid-resistant diamond residue was prepared essentially following standard procedures (Amari et al. 1994): treatment of bulk Murchison using HCl and HF/HCl to dissolve silicates, CS_2 extraction of elemental sulfur, light oxidation using Na dichromate, colloidal extraction in ammonia of nanodiamonds, and finally, cleaning of the diamond fraction by treatment with perchloric acid. Optical and scanning electron microscope (SEM) inspection indicated the dry ($\sim$300 ppm) residue to be rather pure nanodiamond.

As the isotopic results presented below suggest the presence of substantial amounts of *s*-process elements, we gave a small portion to A.B. Verchovsky (Open University, Milton Keynes) to check for the abundance of SiC by stepwise combustion and isotopic analysis of C. The resulting abundance is 2% of SiC in the diamond residue, or 6 ppm relative to bulk Murchison. Since there is also a SiC fraction (unweighed to avoid loss of material), the result confirms that the abundance of SiC in Murchison is substantially larger than the $\sim$6 ppm value inferred by Amari et al. (1994). Possibly it is on the order of 30 ppm, as suggested by Ott & Merchel (2000) based on noble gas results for a chemically minimally treated sample, or even >150 ppm as suggested by the "gentle separation" observations of Tizard et al. (2005). While having a not-so-pure sample of SiC for this work may not have been ideal in all respects, SiC (as discussed in § 3.2) accounts for the bulk of the elements of interest, and having a $\sim$50 times larger sample clearly facilitated handling.

2.2. *Mass Spectrometric Analysis*

Our approach to mass spectrometric analysis has been defined by the attempt to cover as wide a range of elements as possible. The following facts were also taken into account: (1) expected effects are large in presolar grains, and (2) amounts of material available for analyses are small. Measurements were done at Rice University using a high-sensitivity, high-resolution ICP-MS ThermoFinnigan Element II. This single collector reverse-geometry magnetic sector instrument is characterized by high sensitivity ($\sim 3 \times 10^6$ Hz on a ng/g solution), high scan speed, and high mass resolution capabilities ($m/\Delta m = 4000$–$20{,}000$). Ba and REEs were determined in low resolution ($m/\Delta m = 300$) in order to maximize sensitivity. For masses below 100 amu, measurements were done in medium resolution ($m/\Delta m = 3{,}000$). The latter data will be reported separately elsewhere and are not discussed here. Scans were done by changing the voltage on the electrostatic analyzer for a given magnet current. Over the mass range of interest, the magnetic current was changed three times because the electrostatic mass range at a given current is only $\sim$12%. Magnet settling times were 0.01 s, while total peak duration was 0.1 s; 30 scans were made.

For analysis, the diamond/SiC residue was suspended in ammonia. The suspension was free aspirated through a Teflon micronebulizer (Elemental Scientific) at an uptake rate of 10 μL minute^{-1} into a borosilicate glass cyclonic spray chamber followed by introduction into the plasma torch of the mass spectrometer. At plasma temperatures of 7000–8000 K (forward power of 1200 W) the grains were vaporized and most of its constituents ionized.

Altogether three sample analyses were performed, first on a split (named "Mur old") taken from the dry bulk residue, and several months later two analyses (Mur 1 and Mur 2) on a second split. To check the performance we also performed two analyses of terrestrial artificial diamonds ("Rice diamonds"; EXTEC Corporation water-based diamond slurry for polishing, 0.1 μm) under the same experimental conditions. However, for many trace elements abundances were too low in the terrestrial diamond slurry, and no meaningful results were obtained. We have also analyzed a basalt standard solution BIR 1 in 2% HNO_3 (USGS standard) using the same measurement routine. BIR 1 data were used to calibrate elemental abundance ratios in order to account for elemental differences in ionization efficiency and ion transmission. BIR 1 data, however, cannot be used to obtain accurate absolute abundances of presolar grain aggregates due to strong matrix differences.

In most cases isotopic ratios (with 1 σ errors) were obtained from the raw signals by averaging the isotopic ratios calculated from the results of individual scans (usually 30). In cases with very small signal, the counts from the individual scans were added up and ratios calculated from the sums. Signals were fluctuating to some extent (with some bursts) and obvious outliers were eliminated before data reduction. Ammonia blanks were run on solution without suspended sample before and after sample analyses. The average blank background signal intensities were subtracted from the intensities measured on samples. Mass fractionation was corrected for by assuming $1.5\% \pm 1.0\%$ amu^{-1} fractionation favoring the heavy isotopes (this was estimated from observed fractionations seen in BIR 1, having normal isotopic compositions). Interferences were a problem; ratios are reported only where there are no significant isobaric interferences or where corrections could be applied with sufficient confidence. Specific details of interference corrections are discussed for each case in § 3.1.

3. RESULTS AND DISCUSSION

3.1. *Isotopic Compositions*

Results are summarized in Table 1, which gives the measured isotopic compositions after appropriate corrections, the normal isotopic ratios ("best measurement from a single terrestrial source"; de Laeter et al. 2003), and theoretical ratios produced by the *s*-process calculated from the yields given in Arlandini et al. (1999) for their stellar model. Most measured ratios can be explained by a mixture between normal and pure *s*-process, typically in a ratio $\sim$1:2. Since corrections for isobaric interferences involved in a number of ratios listed in Table 1 were not always straightforward, we discuss the various elements and the reliability of the data in detail below. Errors associated with these correction procedures are somewhat arbitrary. Special emphasis is given to cases where previous measurements by other techniques were not fully in agreement with model predictions.

Barium.—Barium spectra are compromised by the presence of Xe impurities in the Ar plasma of the ICP-MS, which made it impossible to obtain data for the rare *p*-process-only isotopes ^{130}Ba and ^{132}Ba. Corrections were applied to ^{134}Ba and ^{136}Ba based on the ^{132}Xe signal, assuming normal atmospheric Xe

TABLE 1
Isotopic Abundance Ratios in Murchison SiC Compared with Normal and *s*-Process Composition

Isotope or Ratio	Mur Old	Mur 1	Mur 2	Normal[c]	*s*-Process[d]
^{136}Ba	127000	10400	7700		
^{134}Ba/^{136}Ba	0.316(8)	0.338(56)	0.331(62)	0.3078	0.302
^{135}Ba/^{136}Ba	0.775(9)	0.324(17)	0.387(18)	0.8394	0.219
^{137}Ba/^{136}Ba	1.340(16)	0.880(50)	0.935(42)	1.4303	0.933
^{138}Ba/^{136}Ba	8.58(19)[a]	6.95(40)	7.05(30)	9.130	7.80
^{144}Nd	4870	3000	2070		
^{142}Nd/^{144}Nd	1.90(10)	2.08(8)	2.06(15)	1.1397	2.08
^{143}Nd/^{144}Nd	0.403(13)	0.432(30)	0.395(18)	0.5111	0.316
^{145}Nd/^{144}Nd	0.217(8)	0.228(20)	0.227(16)	0.3483	0.189
^{146}Nd/^{144}Nd	0.798(25)	0.777(40)	0.785(40)	0.7205	0.911
^{149}Sm	194	139	105		
^{147}Sm/^{149}Sm	1.39(16)	1.11(18)	1.03(23)	1.0850	1.85
^{152}Sm/^{149}Sm	3.09(40)	1.80(30)	1.85(30)	1.9352	3.55
^{153}Eu	306	67	45		
^{151}Eu/^{153}Eu[b]	0.55(20)	1.16(45)	0.20(51)	0.9161	1.18
^{158}Gd	1950	1890	1070		
^{157}Gd/^{158}Gd	0.419(23)	0.410(25)	0.349(35)	0.6302	0.246
^{162}Dy	1400	913	567		
^{161}Dy/^{162}Dy	0.479(22)	0.499(32)	0.477(33)	0.7415	0.251
^{163}Dy/^{162}Dy	0.561(22)	0.435(27)	0.473(28)	0.9773	0.215
^{164}Dy/^{162}Dy	1.20(8)	1.17(8)	1.08(12)	1.1093	1.59
^{168}Er	1500	782	549		
^{166}Er/^{168}Er	0.750(31)	0.850(44)	0.910(65)	1.2415	0.658
^{167}Er/^{168}Er	0.403(22)	0.447(26)	0.447(29)	0.8476	0.259
^{170}Er/^{168}Er	0.245(70)	0.284(35)	0.245(80)	0.5522	0.142
^{172}Yb	65	60	24		
^{171}Yb/^{172}Yb	0.67(14)	0.45(13)	0.86(27)	0.6541	0.299
^{173}Yb/^{172}Yb	1.05(37)	0.47(24)	0.80(55)	0.7389	0.519
^{178}Hf	34100	14400	11700		
^{176}Hf/^{178}Hf	0.211(5)	0.210(5)	0.204(6)	0.1928	0.319
^{177}Hf/^{178}Hf	0.668(8)	0.655(8)	0.660(11)	0.6788	0.220
^{179}Hf/^{178}Hf	0.484(6)	0.491(9)	0.490(9)	0.4993	0.323
^{180}Hf/^{178}Hf	1.342(40)	1.316(32)	1.271(32)	1.2859	1.70

Note.—For discussion of measured values and uncertainties due to interferences see text. Also shown are signal intensities (in hertz) of the normalizing isotopes.

[a] Additional uncertainty due to high intensity on ion counter.

[b] Possibly compromised by BaO interference.

[c] De Laeter et al. (2003), best measurement from a single terrestrial source.

[d] Calculated from yields in the stellar model of Arlandini et al. (1999).

composition and (as assumed for all elements throughout this work) mass fractionation of $1.0\% \pm 0.5\%$ amu^{-1}, favoring the heavy isotopes. Corrections to ^{134}Ba were still substantial but much smaller at ^{136}Ba, where the uncertainty introduced from the corrections was less than 3% for all three samples. While there are no interfering isobars at masses 135 and 137, there are in principle additional interferences at mass 136 from Ce and at mass 138 from La and Ce. These are, however, rare isotopes of La and Ce, which in turn, are much less abundant than Ba in our samples; their possible contribution can be safely neglected, amounting to less than 1% when using even the most unfavorable assumptions.

As for the ^{138}Ba/^{136}Ba ratio there is an additional source of error, which could only roughly be estimated, because of the relatively large beam of ^{138}Ba to which the ion counter was exposed, giving rise to dead time effects. Within the overall uncertainties, however, in a plot of ^{138}Ba/^{136}Ba versus ^{135}Ba/^{136}Ba the data points plot close to the mixing line between normal Ba and *s*-process Ba as derived from previous TIMS measurements (Ott & Begemann 1990a; Prombo et al. 1993). They plot below the line joining normal composition with the *s*-process composition given by the stellar model of Arlandini et al. (1999), which tries to reproduce the *s*-process pattern characteristic of solar system material. This is because of the sensitivity of the yield for closed neutron shell ^{138}Ba to neutron exposure and the well-known fact that the *s*-process documented in presolar SiC grains is characterized by a neutron exposure only about half that characteristic for the *s*-process contribution to the solar system (Ott & Begemann 1990a; Gallino et al. 1993). In a plot of ^{137}Ba/^{136}Ba versus ^{135}Ba/^{136}Ba (Fig. 1) our data confirm the previously observed discrepancy between TIMS data and model expectation (Ott & Begemann 1990a; Gallino et al. 1993). In ^{134}Ba/^{136}Ba the error after correction for Xe interference is too large to make a meaningful statement.

Neodymium.—For Neodymium, as for Ba, relatively precise previous data on bulk SiC exist from previous TIMS measurements; at present, however, unlike for Ba, there are no single grain data by RIMS or SIMS. Isobaric interferences exist at masses 142 from Ce and at masses 144, 148, and 150 from Sm. No data are given in Table 1 for ^{148}Nd and ^{150}Nd. The latter is an *r*-only isotope, and ^{148}Nd also almost so, while the corresponding Sm isotopes are essentially *s*-only, so corrections to Nd in these cases are too large and dependent on the relative amounts of normal and pure *s*-process Sm. In contrast, ^{144}Sm is *p*-only, and corrections,

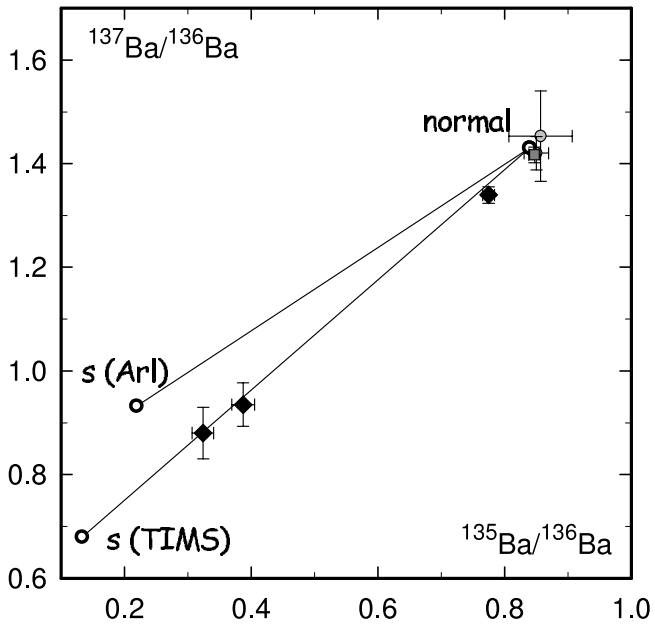

FIG. 1.—Three-isotope plot $^{137}Ba/^{136}Ba$ vs. $^{135}Ba/^{136}Ba$. The measured data (*diamonds*) plot on a mixing line between normal composition (de Laeter et al. 2003) and the *s*-process composition as derived from previous TIMS work (Ott & Begemann 1990a; Prombo et al. 1993). Reference compositions (normal, *s*-process according to TIMS, and *s*-process according to the stellar model of Arlandini et al. [1999]) are shown by open circles. The gray symbols show data measured on terrestrial samples (BIR standard, *filled square*; and two measurements of Rice diamond, *filled circles*; see text).

even in the worst case (assuming Sm to have normal isotopic composition), amount to less than 1%.

There may be some unidentified molecular interferences at masses 143 and 145, which possess no true isobars, but are rare isotopes of Nd. In a plot of $^{143}Nd/^{144}Nd$ versus $^{145}Nd/^{144}Nd$ (Fig. 2*a*), the data plot above and to the left of mixing lines between normal and both TIMS-derived and theoretical *s*-process compositions. A similar behavior is also shown by the terrestrial test samples. Since Rh and Pd, as with other noble metals, are quite abundant in acid-resistant residues (Merchel et al. 2003), possible interferences are Rh and Pd argides formed in the Ar plasma of the mass spectrometer. They would, of course, also affect Nd isotopes 142, 144, and 146, but to much lesser extent. Comparing the necessary efficiency of argide formation (~0.1%) with that observed for heavy platinum group elements as analogs, on the other hand, does not support such an interpretation. Signals at mass 236 ($^{196}Pt^{40}Ar$) are only $\sim 10^{-4}$ those at mass 196.

Given that there may be unidentified interferences on the order ~10% at masses 143 and 145, most of our Nd data are in-line with both expectations and previous TIMS data. This is also true for *s*-only ^{142}Nd, which requires major correction for ^{142}Ce that might range between ~3% (for *s*-process Ce) and ~40% (for isotopically normal Ce). The ratios listed in Table 1 assume the contribution of normal Ce at the reference Ce isotope ^{140}Ce to be 15% ± 15%, similar to the mixing ratio implied by the isotopic data for ^{136}Ba (Fig. 1) and ^{144}Nd (Fig. 2). Some discrepancy, however, seems to exist at mass ^{146}Nd, where experimental data, both from TIMS and from our work (even more so after a ~10% correction to ^{145}Nd) indicate $^{146}Nd/^{144}Nd$ to be ~15% lower than theoretical expectations.

Samarium.—Samarium is much less abundant than Nd. Even for the *s*-only isotopes ^{148}Sm and ^{150}Sm corrections for interference from ^{148}Nd and ^{150}Nd are too dependent on the assumed mixing ratio in Nd to arrive at reasonably safe conclusions for Sm. The ratio $^{147}Sm/^{149}Sm$ of the two isotopes that have no isobars has large analytical uncertainty (Table 1) and only in one case (Mur old) is it higher than normal by more than 1 σ. The situation is similar for $^{152}Sm/^{149}Sm$, where after a "reasonable" correction for ^{152}Gd, only Mur old shows a shift toward *s*-process composition. For that correction, based on the $^{157}Gd/^{158}Gd$ ratio (see below), mixing ratios of normal Gd/pure *s*-process Gd at mass 152 of 45/55, 40/60, and 30/70 were used for Mur old, Mur 1, and Mur 2, respectively. In essence, our Sm data do not put constraints on the isotopic composition of *s*-process Sm.

Europium.—Europium has only two isotopes, ^{151}Eu and ^{153}Eu. In the solar system mix of *s*- and *r*-processes, both are dominated

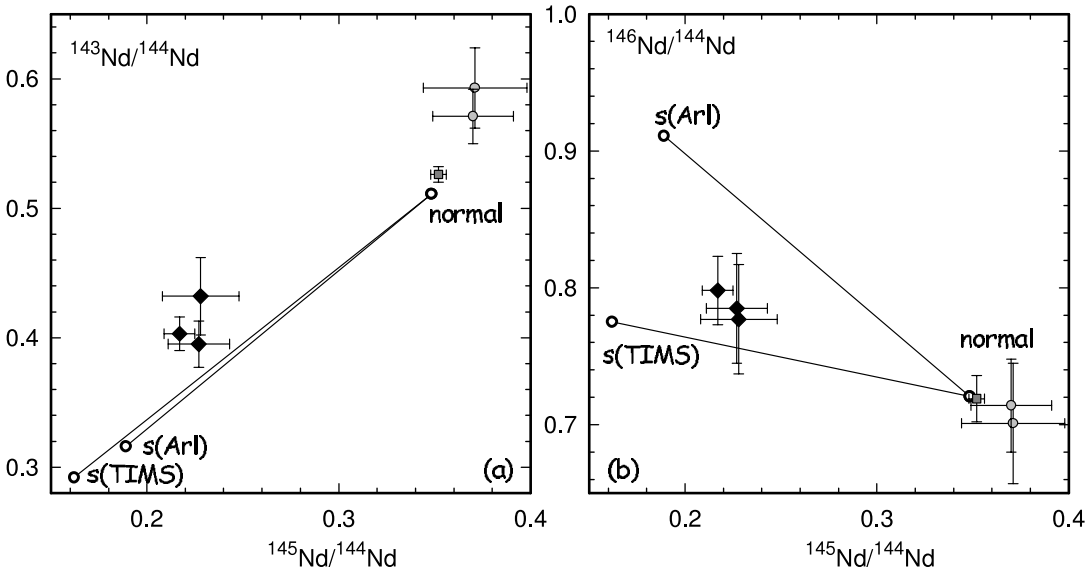

FIG. 2.—Plots of (*a*) $^{143}Nd/^{144}Nd$ and (*b*) $^{146}Nd/^{144}Nd$ vs. $^{145}Nd/^{144}Nd$. Murchison SiC data are filled diamonds. Also shown are mixing lines between normal composition (de Laeter et al. 2003) and both the *s*-process composition according to the stellar model of Arlandini et al. (1999) and as derived from previous TIMS work (summarized in Hoppe & Ott 1997). The gray symbols show data measured on terrestrial samples (the BIR standard, *filled square*; and two measurements of Rice diamond, *filled circles*). See text for discussion.

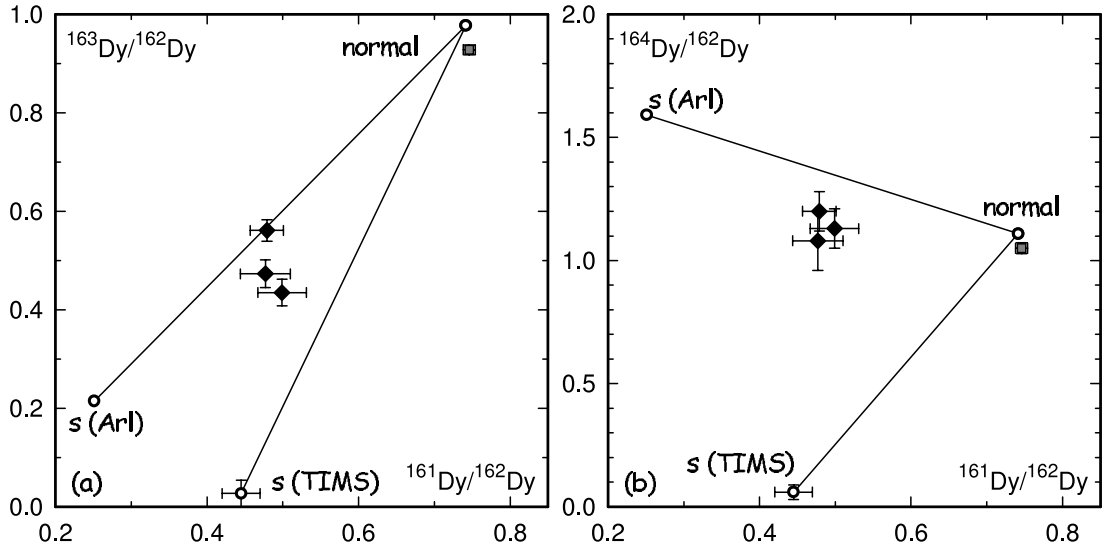

FIG. 3.—Same as Fig. 2, but for (*a*) ^{163}Dy/^{162}Dy and (*b*) ^{164}Dy/^{162}Dy vs. ^{161}Dy/^{162}Dy.

(>90%) by the *r*-process contribution. As a consequence, the Eu abundance in presolar SiC is low. Another complication is the possibility of molecular interferences (oxides) from abundant Ba, although the required efficiency of oxide formation to account for a significant contribution at mass 151 would be rather high (∼1%). In any case, analytical uncertainties are larger than the difference between normal and the expected composition of *s*-process Eu (Table 1); the nominal signal at mass 151 constitutes a safe upper limit to the elemental abundance (§ 3.2).

Gadolinium.—The *s*-process abundance of the lightest isotope ^{152}Gd is of considerable interest for the description of the *s*-process. Because of the temperature-sensitive branching at ^{151}Sm, ^{152}Gd may be the best *s*-process thermometer (Käppeler et al. 1990; Wisshak et al. 1995). Unfortunately, because of the presence of Sm isobars at masses 152 and 154, it is not possible with our approach to derive the abundances of rare ^{152}Gd and ^{154}Gd. Similarly, the abundance of ^{160}Gd cannot be derived with meaningful certainty because of the presence of the *s*-only isobar ^{160}Dy. In addition, masses 155 and 156 are seriously compromised by molecular interferences. Oxides of ^{139}La and ^{140}Ce are possibilities, but with intensities at 155 and 156 being ∼70% of the intensities at masses 139 and 140, this would require unreasonably high levels of oxide formation for these two elements. This would also be in contrast not only to ^{138}Ba but also to chemically similar ^{141}Pr and ^{142}Nd, since there is no evidence at masses 154, 157, and 158 for a similar abundance of Ba, Pr, and Nd oxides. These isotopes seem to be interference-free to first order, and the ^{157}Gd/^{158}Gd ratio (Table 1) is roughly consistent with the "typical" mixing ratio 2:1 for contributions from pure *s*-process versus normal to ^{158}Gd (assuming the Arlandini et al. *s*-process ratio). Assuming a similar mix at ^{162}Dy (cf. Fig. 3) and subtracting the resulting abundance of ^{160}Dy also leads to a consistent inferred ^{160}Gd abundance.

Dysprosium.—The mass range ∼160 to ∼180 is largely free from molecular interferences. Since ^{160}Dy is an *s*-only isotope, it would be preferable to use it as reference isotope. However, precise correction for the abundant isobar ^{160}Gd is difficult, so we have normalized to ^{162}Dy instead in Table 1 and in Figure 3. The abundances of ^{163}Dy and ^{164}Dy are of special interest because of the possibility of bound-state β-decay of ^{163}Dy under stellar conditions, which leads to a branching at ^{163}Dy (Käppeler et al. 1989). Thus the abundances of ^{163}Dy, ^{164}Dy, and ^{164}Er are a measure of the electron density and by inference mass density at the location of the *s*-process (Takahashi & Yokoi 1987; Jaag & Käppeler 1996). Serious disagreement, however, exists between data obtained by TIMS on bulk SiC samples (Richter et al. 1994; Hoppe & Ott 1997) and theoretical expectations (Jaag & Käppeler 1996; Arlandini et al. 1999). The new data obtained in this work are plotted in Figure 3. In the ^{163}Dy/^{162}Dy versus ^{161}Dy/^{162}Dy plot of Figure 3*a*, our data are more in-line with theory than with the TIMS data. This is particularly so if it is taken into account that in analogy to the (low-intensity) terrestrial samples, the SiC data may be slightly shifted to the lower right due to small unidentified interferences. At mass 164, based on observed abundances of isobar-free Dy and Er masses, the signal should largely be from ^{164}Dy, with contributions from ^{164}Er between ∼3% (normal Er composition) and ∼15% (*s*-process composition of Arlandini et al. 1999). Ratios for ^{164}Dy/^{162}Dy listed in Table 1 and plotted in Figure 3*b* again assume a mixing ratio in Er (see also Fig. 4) of 2:1 between pure *s*-process and normal Er, leading to a correction to ^{164}Dy of ∼10%. The corrected data (Fig. 3*b*) seem intermediate between the theoretical and TIMS data. Choosing a different correction to ^{164}Dy within the possible range for contributions from ^{164}Er (see above) does not significantly change this conclusion and the true abundance of *s*-process ^{164}Dy is one of the questions that need to be addressed by future work. Data not corrected for the Er contribution to mass 164 provide upper limits to the ratio (^{164}Dy + ^{164}Er)/^{162}Dy, which are 1.34 ± 0.06, 1.25 ± 0.06, and 1.24 ± 0.08 for Mur Old, Mur 1, and Mur 2, respectively. As for *s*-only ^{160}Dy, it can be shown that using a correction for ^{160}Gd, assuming a 2:1 mixture between pure *s* and normal components (based on ^{157}Gd/^{158}Gd), leads to perfect agreement with the theoretical ^{160}Dy/^{162}Dy ratio.

Erbium.—As noted above, ^{164}Er contributes only little to the intensity at mass 164 and its abundance cannot be inferred from our measured signal. There are no interfering isobars at masses 166 and 167, so these are uncritical; the case of ^{168}Er is similar, since only the extremely rare ^{168}Yb interferes. Because of the general depletion of Yb isotopes (see below), correction for ^{170}Yb is also manageable, amounting to between 2% and 5% of the mass 170 signal in the most favorable case (Mur 2), and between 3% and 11% in the least favorable case (Mur 1) for the extreme assumptions of normal Yb and pure *s*-process Yb. Data listed in Table 1 have been corrected, assuming again a 2:1

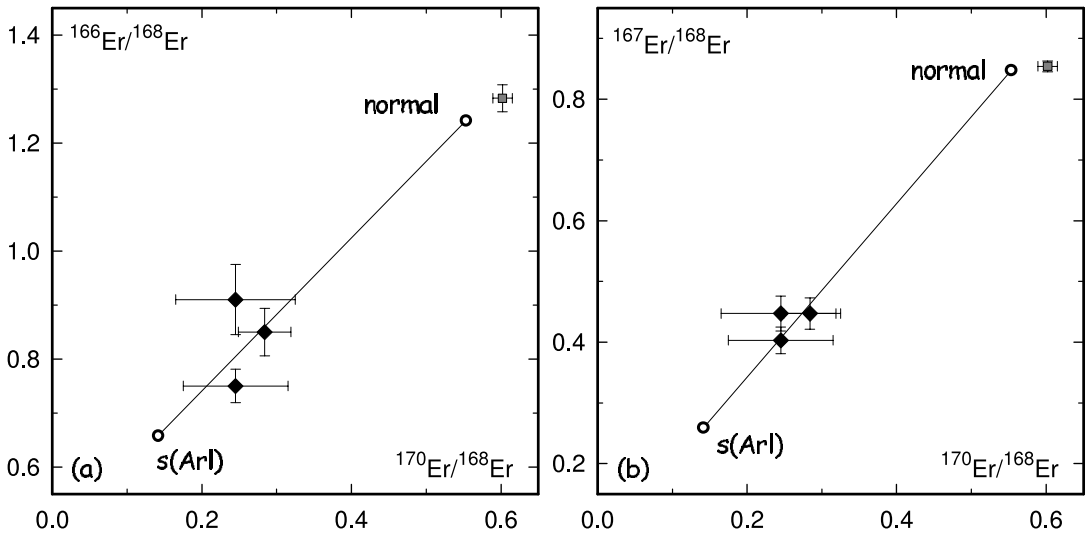

FIG. 4.—Same as Fig. 2, but for (*a*) $^{166}Er/^{168}Er$ and (*b*) $^{167}Er/^{168}Er$ vs. $^{170}Er/^{168}Er$. The Rice diamond samples had too little Er for a meaningful measurement.

mixture; they are plotted as $^{166}Er/^{168}Er$ versus $^{170}Er/^{168}Er$ in Figure 4*a* and as $^{167}Er/^{168}Er$ versus $^{170}Er/^{168}Er$ in Figure 4*b*. In both plots, the data points fall on the mixing line between normal Er and *s*-process Er according to Arlandini et al. (1999).

Ytterbium.—In spite of having no isobars, data for isotopes 171, 172, and 173 have large uncertainties (Table 1), a result of the low ion currents noted above. Isobaric interferences at 168, 170, 174, and 176 swamp the low signals of Yb proper and no data are listed in Table 1.

Hafnium and up.—Starting from Hf and continuing through Ta, W, Re, and the platinum group elements, contributions from acid-resistant phases other than SiC or diamond, like metal nuggets (cf. Merchel et al. 2003), dominate and isotopic compositions are close to isotopically normal within error. Only for Hf is there still a noticeable shift (a few percent) toward the *s*-process composition (Table 1).

Praseodymium, terbium, holmium, thulium.—These are single-isotope elements. However, their abundances still give upper limits to the *s*-process abundances that are used in the discussion of the elemental abundance pattern in § 3.2.

Lanthanum, cerium, lutetium.—The situation is similar for these three elements since the minor isotope(s) are dwarfed in abundance by abundant isobars of Ba, Ba plus Nd, and Hf (plus a little Yb), respectively.

Summary of isotopic observations.—The isotopic signature of the *s*-process has clearly been observed for several elements in the region of Ba and the REE. Our new data obtained by ICP-MS confirm previous analyses by TIMS for Ba and Nd including discrepancies between observations and theoretical expectations in $^{137}Ba/^{136}Ba$ and $^{146}Nd/^{144}Nd$. The signatures observed in dysprosium, on the other hand, are more in line with theory than with previous TIMS measurements. For Er, the *s*-process signature has been observed for the first time and agrees with expectations within error. For several other elements no data were obtained either because of analytical limitations, because they are mono-isotope elements or because of low abundance (see § 3.2 below).

3.2. *Elemental Abundance Patterns*

In contrast to previous measurements that used different mass spectrometric methods, our results provide information not only on isotopic ratios but also on abundance ratios between nuclides of different elements. Before discussing these in detail, we return to the question of whether indeed the *s*-process signatures observed in the isotopic ratios of Ba and the REE are due to the presence of SiC or if they should be ascribed to some other mineral phase. A meaningful estimate can be made for La, and the result by inference should hold for Ba and the other REE as well. To do so, we combine the SiC abundance of ~2% inferred from the carbon isotopes (see § 2) with the average La concentration in presolar SiC as determined by ion probe by E. K. Zinner (reported in Ott et al. 2005a) of ~20 ppm. The resulting "expected" abundance in our samples of ~0.4 ppm is almost twice the upper limit observed by Merchel et al. (2003) in a similar prepared sample (their MKL) from the Murchison meteorite. Hence the "SiC impurity" in our sample can easily account for the bulk of the REE that are present.

The results for the elemental ratios are summarized in Table 2, where nuclide abundance ratios are normalized to ^{144}Nd. The values correspond to the ratios in the "pure *s*-process component" the abundances of which were derived based on the positions of the measured data points on the mixing line between normal and theoretical *s*-process isotopic compositions. This is more reliable than using total abundances because of the possibility of contributions to the totals from sources other than SiC. Relative sensitivities of various elements were obtained from the analysis of the BIR 1 standard (see § 2).

We estimate typical uncertainties of the ratios so derived to be on order 20%–30%, as also indicated from the variation of the results for the three samples (Table 2). They are somewhat higher for Gd and especially Hf; for the latter the obvious reason is that isotopic deviations from normal were only small and hence not as well determined. In addition, for a number of elements only upper limits can be given, because they are either mono-isotopic or dominated by a single isotope (La, Ce, Pr, Tb, Ho, Tm; see end of § 3.1). These are simply based on the total measured abundance. Similarly, upper limits based on total abundance are given for Sm, Eu, and Yb, because partitioning between components was too uncertain.

Also listed in Table 2 are the corresponding abundance ratios as they follow from the stellar model of Arlandini et al. (1999) that tries to reproduce the solar system *s*-process abundance curve. Measured values divided by the Arlandini predictions are plotted in Figure 5*a*. Not shown are those elements for which there

TABLE 2

ABUNDANCE RATIOS OF *s*-PROCESS NUCLIDES OF VARIOUS ELEMENTS IN MURCHISON SiC COMPARED TO ARLANDINI ET AL. (1999) STELLAR MODEL PREDICTIONS FOR SOLAR SYSTEM *s*-PROCESS CONTRIBUTION AND TO A "SIMPLE CLASSICAL" MODEL WITH LOW NEUTRON EXPOSURE

Ratio	Mur old	Mur 1	Mur 2	Arlandini[a]	Simple 0.15[b]
$^{136}Ba/^{144}Nd$	3.2	3.6	3.4	3.54	10.2
$^{139}La/^{144}Nd$	<4.9	<4.0	<4.9	2.77	4.8
$^{140}Ce/^{144}Nd$	<12	<13	<16	8.36	10.4
$^{141}Pr/^{144}Nd$	<1.2	<1.2	<1.3	0.813	0.97
$^{149}Sm/^{144}Nd$	<0.025	<0.013	<0.012	0.0445	0.040
$^{151}Eu/^{144}Nd$	<0.021	<0.018	<0.011	0.0304	0.029[c]
$^{158}Gd/^{144}Nd$	0.17	0.22	0.32	0.225	0.21
$^{159}Tb/^{144}Nd$	<0.16	<0.17	<0.15	0.0436	0.042
$^{162}Dy/^{144}Nd$	0.13	0.19	0.16	0.164	0.14
$^{165}Ho/^{144}Nd$	<0.19	<0.17	<0.16	0.0695	0.048
$^{168}Er/^{144}Nd$	0.20	0.16	0.19	0.190	0.18
$^{169}Tm/^{144}Nd$	<0.046	<0.041	<0.043	0.0503	0.052
$^{172}Yb/^{144}Nd$	<0.043	<0.016	<0.0020	0.165	0.17
$^{178}Hf/^{144}Nd$	0.2	0.1	0.3	0.240	0.17

NOTE.—For a detailed discussion of measured values and uncertainties see text. The normalizing nuclide is ^{144}Nd.

[a] According to the stellar model of Arlandini et al. (1999).

[b] Calculated from a simple model (see text), assuming a neutron exposure $\tau_0 = 0.15$ mbarn^{-1} and using the Maxwellian-averaged cross sections of Bao et al. (2000).

[c] From ^{153}Eu prediction of simple model and $^{151}Eu/^{153}Eu$ ratio of stellar model.

are upper limits only (Table 2) because of being mono-isotopic (Tb, Ho, Tm) or nearly so (La, Ce, Pr). Remarkably, many data points plot near the 1 line, implying agreement between measurement and predictions. Sm, Eu, and, most clearly, Yb, however, show significant deficits.

A problem with the normalization to the Arlandini et al. (1999) predictions is that these try to reproduce the solar system *s*-process pattern. The *s*-process recorded in SiC grains is characterized by an effective neutron exposure; however, that is only about one-half that typical of solar system *s*-process material, a fact evident in the isotopic ratios for Ba as discussed by Ott & Begemann (1990a) and Gallino et al. (1993). For this reason, in Figure 5*b* we also show a comparison of measured abundance ratios with those that follow from a classical model (Käppeler et al. 1989; Arlandini et al. 1999) assuming an exponential distribution of exposures $\rho(\tau) = \tau_0 \exp(-\tau/\tau_0)$ with average neutron exposure $\tau_0 = 0.15$ mbarn^{-1} and using the Maxwellian-averaged capture cross sections of Bao et al. (2000). Our model is a "simplified" one in that it does not follow minor branchings that are not important on the scale of accuracy we are concerned with. In fact, on the scale of Figure 5 predictions from the stellar model of Arlandini et al., their classical model with $\tau_0 = 0.30$ mbarn^{-1}, and "simplified classical models" with $\tau_0 = 0.30$ mbarn^{-1} as well as 0.15 mbarn^{-1} are indistinguishable for the mass range of Nd and above, where neutron capture cross sections are large. The lower 0.15 mbarn^{-1} exposure, however, results in significantly enhanced ratios of the Ba, La, Ce, and Pr nuclides relative to Nd (Table 2), a consequence of the closed

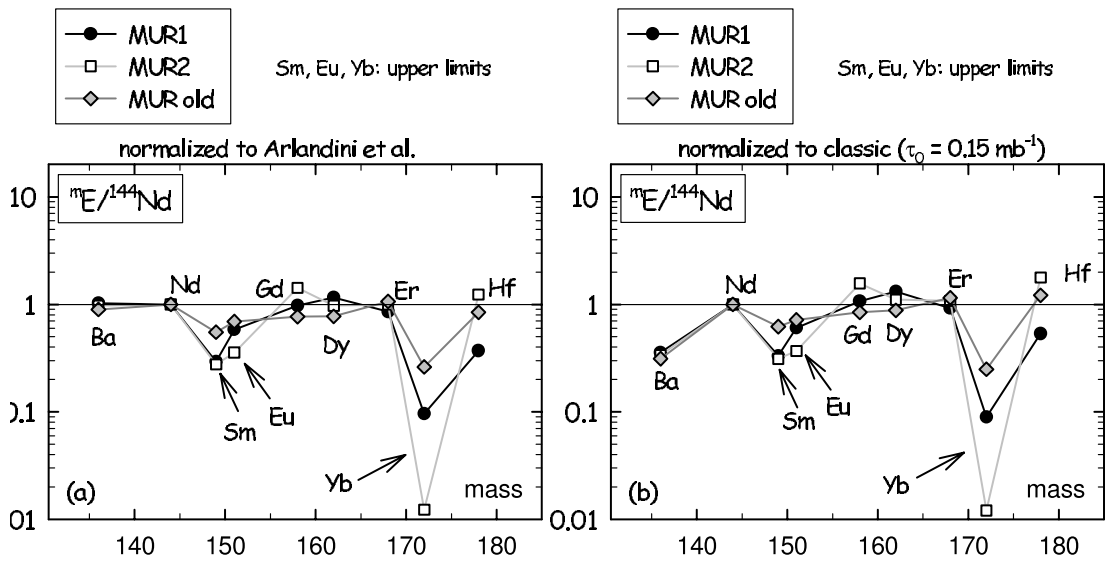

FIG. 5.—Abundance ratios of *s*-process nuclides in Murchison SiC in the range from Ba through Hf, normalized to ^{144}Nd. Not shown are those elements for which there are upper limits only (Table 2) because they are mono-isotopic (Tb, Ho, Tm) or nearly so (La, Ce, Pr). (*a*) Normalized to ratios calculated from the stellar model of Arlandini et al. (1999). (*b*) Normalized to expectations from a simplified classical model with neutron exposure $\tau_0 = 0.15$ mbarn^{-1}. On the scale of these graphs, there is little difference between the models in the mass range above Nd (where neutron capture cross sections are large). See text for detailed discussion.

$N = 82$ neutron shell and the correspondingly small capture cross sections of ^{138}Ba, ^{139}La, ^{140}Ce, ^{141}Pr, and ^{142}Nd.

As a result, the major difference between the patterns in Figures 5*a* and 5*b* is that in Figure 5*b* Ba/Nd is low (by a factor $\sim$3) relative to the prediction. Similarly, overabundances of La, Ce and Pr are lower (Table 2), consistent with roughly equal mixing ratios between pure *s*-process and normal component for the elements from Ba to Nd (as well as Gd, Dy, and Er among the higher masses). As for elemental ratios in the *s*-process component, the main conclusion from Figure 5*b* and Table 2 is that most are consistent with the production ratios except for Ba, Sm, Eu, most clearly Yb, and possibly mono-isotopic Tm, for which we have an upper limit only. Interestingly, these are the elements among those we have investigated that are the most volatile and expected to condense last from the vapor phase into SiC grains.

Because of their otherwise similar chemical properties, the abundance of the REEs is a useful tool in cosmochemistry to infer redox conditions and volatility-related effects, e.g., in Ca-Al–rich inclusions (MacPherson et al. 1988) or chondrules (Pack et al. 2004). Their condensation behavior in a reducing environment with otherwise solar abundances has been studied by Lodders & Fegley (1993), who also studied the condensation behavior of a whole range of trace elements for the specific case of condensation around carbon stars (Lodders & Fegley 1995, 1997). Unfortunately this dedicated work reports results for the lightest of the REEs only, La in some cases, in addition Ce and Nd in some others. Nevertheless, a few general statements are possible based on the results of their work.

Initially, as in the reducing but otherwise solar environment of Lodders & Fegley (1993), Ba and the REEs are expected to condense in carbon star atmospheres as sulfides, at temperatures below the condensation temperature of SiC (cf. BaS and LaS in Table 7 of Lodders & Fegley 1995). These sulfides condense into the preexisting SiC, where they form solid solutions. Condensation temperatures under conditions of solid solution formation with SiC are increased as compared to the case of simple sulfide condensation (Lodders & Fegley 1995), but nevertheless, the relative sequence in the case of pure sulfide condensation or condensation into oldhamite (CaS; Lodders & Fegley 1993) should be a useful guide. According to such calculations, YbS is the most volatile of the REE sulfides by a wide margin, followed by the sulfides of Eu, Sm, and Tm, with much smaller differences in condensation temperature compared to the bulk of the REE sulfides. This is exactly the pattern that we see in Figure 5*b* in the comparison between observed element ratios and corresponding production ratios. A straightforward interpretation, therefore, is that REEs in the bulk of the presolar SiC grains were produced in abundance ratios as predicted by *s*-process nucleosynthesis models and condensed/incorporated into SiC at a temperature too high for the most volatile of them to be fully incorporated. Dedicated calculations such as those of Lodders & Fegley (1995, 1997) but covering the full REE range could be used in principle to define an exact condensation temperature from this pattern (for a given pressure).

Two puzzles remain. First is the position in Figure 5*b* of Ba, which is expected to be even more volatile than the most volatile of the REEs, but shows a depletion relative to Nd of a factor $\sim$3 only, much less than Yb and maybe also less than Sm and Eu. The only feasible solution may be an additional source for Ba. This could be a source highly enriched in Ba because of precondensed and removed REEs. Alternatively, it could be introduction of part of the *s*-process material by another process favoring Ba over REEs, e.g., ion implantation because of the lower ionization potential and higher expected degree of ionization, as advocated by Verchovsky et al. (2004). Note that ion implantation is the favored mechanism for introducing the noble gases into SiC grains (Lewis et al. 1990; Verchovsky et al. 2004). Notable is also the fact that *single* grain analyses seem to indicate large grain-to-grain variations in the Ce/Nd ratio (Amari et al. 1995) and possibly also in the heavier REEs (Ott et al. 2005b), in spite of the basic close agreement of *bulk* SiC ratios with production ratios. Large variations in elemental ratios have been observed by Amari et al. (1995) in other elements as well, but there they could be attributed to volatility effects; sometimes the more volatile elements were underabundant, sometimes the extremely refractory ones were, probably due to precondensation. No significant volatility difference, however, is expected between Ce and Nd, both refractory REEs under reducing conditions (Lodders & Fegley 1993). Nor does the *s*-process seem capable of producing large variations in Ce/Nd, two neighboring elements. Further single grain analyses including the isotopic composition of REEs may help shed light on this puzzle.

4. CONCLUSIONS

Using a novel technique, ICP mass spectrometric analysis of a suspension of presolar grains, we have determined the compositions of trace elements in the Ba to Hf range in bulk (i.e., grain aggregates) of presolar silicon carbide, the majority of which derives from AGB stars. The signature of the *s*-process is obvious. A typical mixing ratio between the pure *s*-process component and isotopically normal matter is $\sim 2:1$. Within the moderate precision of the measurements, most data are compatible with the *s*-process component having isotopic compositions as predicted from the *s*-process nucleosynthesis calculations of Arlandini et al. (1999). Exceptions are ^{137}Ba and ^{146}Nd, consistent with previous TIMS work. Our new data for Dy, on the other hand, are more in-line with model predictions than with earlier discrepant analytical results obtained by TIMS.

The overall elemental pattern in the mass range of Ba and the rare earth elements is compatible with production ratios as predicted, augmented by the effect of volatility leading to relative deficits in Ba, Sm, Eu, possibly Tm, and most strikingly, Yb. These results should help to better constrain typical conditions during condensation of SiC grains. The close agreement with production ratios is surprising, however, in view of evidence for large grain-to-grain variation of elemental abundance ratios.

We are grateful to Sasha Verchovsky for C analysis of our sample as a means of estimating its SiC content and to Roberto Gallino for fruitful discussions. Ch. Sudek performed the chemical extraction of the Murchison acid-resistant residue. Q. Z. Y. acknowledges NASA Origins of Solar Systems Program for support (NNG05GN03G).

REFERENCES

Amari, S., Hoppe, P., Zinner, E., & Lewis, R. S. 1995, Meteoritics, 30, 679
Amari, S., Lewis, R. S., & Anders, E. 1994, Geochim. Cosmochim. Acta, 58, 459
Anders, E., & Zinner, E. 1993, Meteoritics, 28, 490
Arlandini, C., Käppeler, F., Wisshak, K., Gallino, R., Lugaro, M., Busso, M., & Straniero, O. 1999, ApJ, 525, 886
Bao, Z. Y., Beer, H., Käppeler, F., Voss, F., Wisshak, K., & Rauscher, T. 2000, At. Data Nucl. Data Tables, 76, 70

Bernatowicz, T. J., & Zinner, E., ed. 1997, AIP Conf. Proc. 402, Astrophysical Implications of the Laboratory Study of Presolar Materials (New York: AIP)
de Laeter, J. R., Böhlke, J. K., De Bièvre, P., Hidaka, H., Peiser, H. S., Rosman, K. J. R., & Taylor, P. D. P. 2003, Pure Appl. Chem., 75, 683
Draine, B. T. 2003, ARA&A, 41, 241
Gallino, R., Raiteri, C. M., & Busso, M. 1993, ApJ, 410, 400
Hoppe, P., & Ott, U. 1997, in AIP Conf. Proc. 402, Astrophysical Implications of the Laboratory Study of Presolar Materials, ed. T. J. Bernatowicz & E. Zinner (New York: AIP), 27
Hoppe, P., Ott, U., & Lugmair, G. W. 2004, NewA Rev., 48, 171
Jaag, S., & Käppeler, F. 1996, ApJ, 464, 874
Käppeler, F., Beer, H., & Wisshak, K. 1989, Rep. Prog. Phys., 52, 945
Käppeler, F., Gallino, R., Busso, M., Picchio, G., & Raiteri, C. M. 1990, ApJ, 354, 630
Lewis, R. S., Amari, S., & Anders, E. 1990, Nature, 348, 293
Lodders, K., & Fegley, B., Jr. 1993, Earth Planet. Sci. Lett., 117, 125
———. 1995, Meteoritics, 30, 661
———. 1997, in AIP Conf. Proc. 402, Astrophysical Implications of the Laboratory Study of Presolar Materials, ed. T. J. Bernatowicz & E. Zinner (New York: AIP), 391
MacPherson, G. J., Wark, D. A., & Armstrong, J. T. 1988, in Meteorites and the Early Solar System, ed. J. F. Kerridge & M. S. Matthews (Tucson: Univ. Arizona Press), 746
Marhas, K. K., Hoppe, P., & Ott, U. 2003, Meteoritics Planet. Sci., 38, 5101
———. 2005, Lunar and Planetary Sci. Conf., 36, 1855
Merchel, S., Ott, U., Herrmann, S., Spettel, B., Faestermann, Th., Knie, K., Korschinek, G., Rugel, G., & Wallner, A. 2003, Geochim. Cosmochim. Acta, 67, 4949
Messenger, S., Keller, L. P., Stadermann, F. J., Walker, R. M., & Zinner, E. 2003, Science, 300, 105
Mostefaoui, S., & Hoppe, P. 2004, ApJ, 613, L149
Nguyen, A., & Zinner, E. 2004, Science, 303, 1496
Nicolussi, G. K., Davis, A. M., Pellin, M. J., Lewis, R. S., Clayton, R. N., & Amari, S. 1997, Science, 277, 1281
Nicolussi, G. K., Pellin, M. J., Lewis, R. S., Davis, A. M., Amari, S., & Clayton, R. N. 1998a, Geochim. Cosmochim. Acta, 62, 1093
Nicolussi, G. K., Pellin, M. J., Lewis, R. S., Davis, A. M., Clayton, R. N., & Amari, S. 1998b, Phys. Rev. Lett., 81, 3583
Ott, U. 1993, Nature, 364, 25
Ott, U., Altmaier, A., Herpers, U., Kuhnhenn, J., Merchel, S., Michel, R., & Mohapatra, R. K. 2005a, Meteoritics Planet. Sci., 40, 1635
Ott, U., & Begemann, F. 1990a, ApJ, 353, L57
———. 1990b, in Lunar and Planetary Sci. Conf., 21, 920
Ott, U., & Merchel, S. 2000, Lunar and Planetary Sci. Conf., 31, 1356
Ott, U., Sudek, Ch., Maul, P., Bernhard, P., Elmers, H. J., & Schönhense, G. 2005b, Lunar and Planetary Sci. Conf., 36, 1294
Pack, A., Shelley, J. M. G., & Palme, H. 2004, Science, 303, 997
Prombo, C. A., Podosek, F. A., Amari, S., & Lewis, R. S. 1993, ApJ, 410, 393
Richter, S., Ott, U., & Begemann, F. 1994, Meteoritics, 29, 522
Savina, M. R., Davis, A. M., Tripa, C. E., Pellin, M. J., Clayton, R. N., Lewis, R. S., Amari, S., Gallino, R., & Lugaro, M. 2003, Geochim. Cosmochim. Acta, 67, 3201
Savina, M. R., Davis, A. M., Tripa, C. E., Pellin, M. J., Gallino, R., Lewis, R. S., & Amari, S. 2004, Science, 303, 649
Takahashi, K., & Yokoi, K. 1987, At. Data Nucl. Data Tables, 36, 375
Tizard, J., Lyon, I., & Henkel, T. 2005, Meteoritics Planet. Sci., 40, 335
Verchovsky, A. B., Wright, I. P., & Pillinger, C. T. 2004, ApJ, 607, 611
Whittet, D. C. B. 2003, Dust in the Galactic Environment (2nd ed.; Philadelphia: IOP)
Wisshak, K., Voss, F., Käppeler, F., Guber, K., Kazakov, L., Kornilov, N., Uhl, M., & Reffo, G. 1995, Phys. Rev. C, 52, 2762
Zinner, E. 1998, Annu. Rev. Earth Planet. Sci., 26, 147
Zinner, E., Amari, S., & Lewis, R. S. 1991, ApJ, 382, L47